AIMS Mathematics, 10(3): 5651–5670.
DOI: 10.3934/math.2025261
Received: 08 November 2024
Revised: 06 February 2025
Accepted: 26 February 2025
Published: 13 March 2025

https://www.aimspress.com/journal/Math

Research article

Numerical approximation of the time-fractional regularized long-wave equation emerging in ion acoustic waves in plasma

Hasim Khan, Mohammad Tamsir*, Manoj Singh, Ahmed Hussein Msmali and Mutum Zico Meetei

Department of Mathematics, College of Science, Jazan University, P.O. Box 114, Jazan 45142, Saudi Arabia

* **Correspondence:** Email: mtamsir@jazanu.edu.sa.

Abstract: This work accomplished a novel approximate solution of the time-fractional regularized long-wave (TFRLW) equation. This equation is an appropriate mathematical model in physical sciences that designates the nature of ion acoustic waves in plasma and waves of shallow water. A cubic B-spline (CBS) collocation procedure was used for the spatial discretization, offering greater flexibility and accuracy compared to traditional spline methods. For time discretization, the finite difference method was used, ensuring computational efficiency, while the time-fractional derivative was settled by Caputo's definition. The Rubin-Graves linearization procedure was involved to handle the nonlinear term. To demonstrate the possessions of different constraints and variables on the displacement, the approximate solutions were shown in tabular as well as graphical forms. The method's unconditional stability was confirmed through a detailed von Neumann stability analysis, making it particularly robust for long-term simulations. The order of convergence was also estimated numerically. Three invariant capacities analogous to mass, momentum, and energy were assessed for further justification. Obtained solutions established the exactitude and efficiency of the anticipated method. Furthermore, unlike many existing methods, this approach can be tailored to handle the complexity of higher-order equations while maintaining stability and accuracy over large-scale problems.

Keywords: TFRLW equation; Caputo's fractional derivative; CBS collocation technique; stability analysis; numerical convergence
Mathematics Subject Classification: 35R11, 65M12

1. Introduction

First, Peregrine [1] promulgated the regularized long-wave (RLW) equation to describe the propagation of unidirectional weakly nonlinear dispersive water waves. Furthermore, the authors of [2,3] engaged this equation to illuminate an enormous class of real-world problems as a substitute of the well-known Korteweg–De Vries (KdV) equation. These studies revealed that the RLW equation is more impressive than the latter one. The RLW equation takes part as a fundamental role in the study of the non-linear dispersive waves that have a lot of norms in various precise areas, e.g., magnetohydrodynamic waves as well as ion acoustic plasma waves, longitudinal dispersive and pressure waves in elastic rods and liquid-gas bubble mixtures, and rotating flow down a tube. Bona et al. [4] proposed an integer-ordered formulation of the RLW equation for describing the surface water wave's propagation in a channel.

The RLW equation has been studied by means of numerous procedures. For instance, this equation has been approximated, numerically, by the Galerkin finite element method (FEM) [15,16,34], Petrov-Galerkin FEM [17], least squares FEM [18], CBS and least squares CBS finite element methods (FEMs) [19,25], respectively, least squares quadratic B-spline (QdBS) FEM [20], splitting methods with CBS and QdBS FEMs [21,22], respectively, quintic B-spline Galerkin finite element method (QBS-GFEM) [23], linearized implicit finite difference method (FDM) [24], splitting-up technique with CBS and QdBS [26], quartic B-spline, QBS, and fourth-order CBS collocation techniques [27–29], respectively, CBS differential quadrature method [30], and lumped Galerkin QdBS FEM [33].

It is generally recognized that the trajectory's characteristic of the fractional derivatives is non-local as the remembrance outcome [5]. Many researchers prove that fractional differential equations (FDEs) are more appropriate than integer-order ones, as fractional derivatives demonstrate the memory and inherited possessions of several materials and processes [6–9].

Furthermore, the time-fractional partial differential equations (TFDEs) have generated further consideration for a number of real-life applications such as signal processing, electrical network systems, optics, financial estimation and forecast, mathematical biology, electromagnetic control theory, fluid flows in multi-dimension, material science, acoustics, biological systems associated with predator-prey models, etc. [10–13]. The application of fractional models is rising for enhanced precision in real-life models, and points out substantial necessities for improved fractional mathematical models. In [14], the author implemented Caputo's fractional derivative for dynamical investigation of a generalized tumor model. This derivative is being used for modeling of biological systems, comprising tumor growth. In biomedical research, tumor growth models have been expansively used to examine the dynamics of tumor expansion and estimating possible treatments.

Recently, the TFRLW equation was approximated by some analytical and numerical methods. For instant, the authors of [8] applied a method based on the q-homotopy analysis transform for approximating the TFRLW equation, while in [9], they presented a new fractional extension of the RLW equation. Besides, they used the fixed-point theorem to prove the existence and uniqueness of the solutions. Nikan et al. [35] obtained the traveling-wave solutions of the TFRLW equation using the radial basis function (RBF) collocation technique. Maarouf et al. [38] systematically examined the Lie group analysis technique of the TFRLW equation with the Riemann-Liouville fractional derivative. Naeem et al. [39] developed numerical methodologies that use the Yang transform, the homotopy perturbation method (HPM), and the Adomian decomposition method (ADM) to analyze this equation.

The TFRLW equation is one of the most substantial nonlinear evolution equations used to model various physical phenomena such as ion-acoustic plasma waves, shallow water waves, and

longitudinal waves in elastic rods. Hossain et al. [40] used a modified simple equation integral technique in the TFRLW equation to create kink waves, anti-kink waves, brilliant and dark bell waves, double periodic waves, and combinations of solitons and periodic waves. The fractional RLW equations were used to mathematically model the nonlinear waves in the ocean, and similarly, the fractional RLW equations are used to describe the huge ocean waves known as tsunamis [41]. According to [42], the TFRLW equation can be used to study many phenomena such as plasma waves in complex media, water wave propagation in shallow water, and long-wave occupancy dynamics in the ocean, including tsunamis and tidal waves. Results in [43] can aid in understanding ion-acoustic waves in plasma, shallow water waves in oceans, and the development of a three-dimensional wave packet with finite depth on water under weak nonlinearity using the TFRLW. In [44], the authors obtained the soliton and periodic wave solutions for the TFRLW, which is the first step toward understanding ocean models' structural and physical behavior and coastal and harbor regions of the oceans. The Kudryashov approach was used to investigate the TFRLW problem in [45], which has prospective applications in applied science, nonlinear dynamics, mathematical physics, and engineering and is also important in biosciences, neurosciences, plasma physics, geochemistry, and fluid mechanics.

The most important part of this work is that the Caputo fractional derivative is used in the RLW equation for analyzing the nature of the displacement of shallow-water waves and ion acoustic plasma waves. It takes a broad view of the RLW equation for interpretation of the water waves. In interpretation of the excessive significance of fractional derivatives, we consider a TFRLW equation emerging in ion acoustic plasma waves (1). We use the cubic CBS collocation procedure to discretize the spatial derivatives. The Caputo's definition is used for time-fractional derivative.

$$\frac{\partial^{\alpha} w}{\partial \tau^{\alpha}}+\hat{\gamma}\frac{\partial w}{\partial \zeta}+\hat{\beta}w^{p}\frac{\partial w}{\partial \zeta}-\hat{\mu}\frac{\partial^{3} w}{\partial \zeta^{2}\partial \tau}=f(\zeta,\tau),\ a\le\zeta\le b,\ 0<\alpha<1, \tag{1}$$

with the initial and boundary conditions

$$w(\zeta,0)=\phi(\zeta), \tag{2}$$

$$w(a,\tau)=\psi_{1}(\tau),\ \mathrm{w}(b,\tau)=\psi_{2}(\tau), \tag{3}$$

where p is a positive integer, $\hat{\gamma}$, $\hat{\beta}$ and dissipative term $\hat{\mu}$ are positive constants, $w(\zeta,\tau)$ represents the vertical displacement of the water surface, and the function $f(\zeta,\tau)$ denotes a source term. The notation $\frac{\partial^{\alpha} w}{\partial \tau^{\alpha}}$ indicates the Caputo's time-fractional derivative as

$$\frac{\partial^{\alpha} w}{\partial \tau^{\alpha}}=\begin{cases}\dfrac{1}{\Gamma(1-\alpha)}\displaystyle\int_{0}^{\tau}(\tau-\upsilon)^{-\alpha}\frac{\partial w(\zeta,\upsilon)}{\partial \upsilon}d\upsilon, & 0<\alpha<1\\ \dfrac{\partial w(\zeta,\tau)}{\partial \tau}, & \alpha=1\end{cases}. \tag{4}$$

Definition 1.1. Caputo's integral and derivative of $g(\tau)\in\mathbb{R}$ of order $\alpha\ge 0$ are, respectively, defined by

$${}^{c}J_{0,\tau}^{\alpha}g(\tau)=\frac{1}{\Gamma(\alpha)}\int_{0}^{\tau}(\tau-\xi)^{\alpha-1}g(\xi)d\xi,\ \alpha>0,\ \tau>0,$$

and

$$ {}^{c}D_{0,\tau}^{\alpha} g(\tau) = \frac{1}{\Gamma(\bar{k}-\alpha)} \int_0^{\tau} (\tau - \xi)^{\bar{k}-\alpha-1} g^{(\bar{k})}(\xi) d\xi, \ \tau > 0, \ \bar{k}-1 < \alpha < \bar{k} \in \mathbb{Z}^+ . $$

2. Discretization of the TFRLW equation

This part implements the discretization process of the TFRLW equation by means of the CBS collocation procedure. First, we fix an identical partition of $[0, T]$ with size $\Delta\tau = \frac{T}{N}$, where N is the partition's number of the time variable. Now, we discretize the fractional derivative $\frac{\partial^{\alpha} w}{\partial \tau^{\alpha}}$ for $0 < \alpha < 1$ at $\tau = \tau_{j+1}$ by the $L1$ formula [20,30,31] as follows:

$$ \frac{\partial^{\alpha} w_i^{j+1}}{\partial \tau^{\alpha}} = a_0 \sum_{k=0}^{j} \chi_k \left(w_i^{j+1-k} - w_i^{j-k} \right) + \hat{\delta}^{j+1}, \ \ j = 0,1,2....N, \tag{5} $$

where $a_0 = \frac{\Delta\tau^{-\alpha}}{\Gamma(2-\alpha)}$, $\chi_l = (l+1)^{1-\alpha} - l^{1-\alpha}$, $j = 0,1,\ldots,N$, and $\hat{\delta}^{j+1}$ is the truncate error termed by $\hat{\delta}^{j+1} \le L_w \Delta\tau^{2-\alpha}$, where the constant L_w is associated to w.

Lemma 2.1. The element χ_k, arising in Eq (5), fulfils the following possessions:

$$ \begin{cases} \chi_k > 0, \ k = 0,1,...,N, \\ 1 = \chi_0 > \chi_1 > \chi_2 > ... > \chi_N, \ \chi_N \to 0 \text{ as } N \to \infty \end{cases}. $$

Next, the CBS collocation procedure is used to discretize derivatives of the spatial variable. The domain [a,b] is apportioned consistently with $h = \Delta\zeta = \frac{b-a}{M}$ by $\zeta_i = a + ih$, $i = 0,1,\ldots,M$, such that $a = \zeta_0 < \zeta_1 < \zeta_2 < \ldots < \zeta_M = b$. Now, we define CBS functions $\Upsilon_i(x)$ for $i = -1, \ 0, \ ..., \ M+1$ as:

$$ \Upsilon_i(\zeta) = \frac{1}{h^3} \begin{cases} (\zeta - \zeta_{i-2})^3, & \zeta \in [\zeta_{i-2}, \zeta_{i-1}) \\ (\zeta - \zeta_{i-2})^3 - 4(\zeta - \zeta_{i-1})^3, & \zeta \in [\zeta_{i-1}, \zeta_i) \\ (\zeta_{i+2} - \zeta)^3 - 4(\zeta_{i+1} - \zeta)^3, & \zeta \in [\zeta_i, \zeta_{i+1}) \\ (\zeta_{i+2} - \zeta)^3, & \zeta \in [\zeta_{i+1}, \zeta_{i+2}) \\ 0, & \text{otherwise,} \end{cases}, \tag{6} $$

where $\{\Upsilon_0, \Upsilon_1, ..., \Upsilon_M, \Upsilon_{M+1}\}$ are preferred so that they form a basis over $[a,b]$. The $\Upsilon_i(\zeta)$, $\Upsilon_i'(\zeta)$, and $\Upsilon_i''(\zeta)$ at knot points are valued by the subsequent table (see Table 1).

Table 1. The values of $\Upsilon_i(\zeta)$, $\Upsilon_i'(\zeta)$, and $\Upsilon_i''(\zeta)$ at knots.

	ζ_{i-2}	ζ_{i-1}	ζ_i	ζ_{i+1}	ζ_{i+2}
$\Upsilon_i(\zeta)$	0	σ_1	σ_2	σ_1	0
$\Upsilon_i'(\zeta)$	0	σ_3	0	$-\sigma_3$	0
$\Upsilon_i''(\zeta)$	0	σ_4	$-2\sigma_4$	σ_4	0

where $\sigma_1 = 1$, $\sigma_2 = 4$, $\sigma_3 = \frac{1}{h}$, and $\sigma_4 = \frac{6}{h^2}$. We define the approximate solutions as

$$w(\zeta, \tau_j) \approx \sum_{i=-1}^{M+1} \Upsilon_i(\zeta) C_i(\tau_j), \; j = 0,1,\ldots,N, \tag{7}$$

where $C_i(\tau_j)$ are unknown extents. The variation of $w(\zeta, \tau_j)$ is defined by

$$w(\zeta, \tau_j) = \sum_{m=i-1}^{i+1} \Upsilon_m(\zeta) C_m(\tau_j), \; j = 0,1,\ldots,N. \tag{8}$$

Using Eq (8), we approximate w and its first-and second-order derivatives w_ζ and $w_{\zeta\zeta}$, respectively, with respect to ζ as

$$w_i^j = \sigma_1 C_{i-1}^j + \sigma_2 C_i^j + \sigma_1 C_{i+1}^j, \tag{9}$$

$$(w_\zeta)_i^j = -\sigma_3 C_{i-1}^j + \sigma_3 C_{i+1}^j, \tag{10}$$

and

$$(w_{\zeta\zeta})_i^j = \sigma_4 C_{i-1}^j - 2\sigma_4 C_i^j + \sigma_4 C_{i+1}^j. \tag{11}$$

At $\tau = \tau_{j+1}$, using the Eq (5) for $\frac{\partial^\alpha w}{\partial \tau^\alpha}$ and the θ scheme, we discretize problem (1) as

$$a_0 \sum_{k=0}^{j} \chi_k \left(w_i^{j-k+1} - w_i^{j-k} \right) + \theta\, \hat{\gamma} \left(w_\zeta \right)_i^{j+1} + (1-\theta) \hat{\gamma} \left(w_\zeta \right)_i^{j} + \theta\, \hat{\beta} \left(w^p w_\zeta \right)_i^{j+1} +$$

$$(1-\theta) \hat{\beta} \left(w^p w_\zeta \right)_i^{j} - \hat{\mu} \frac{\left(w_{\zeta\zeta} \right)_i^{j+1} - \left(w_{\zeta\zeta} \right)_i^{j}}{\Delta \tau} = f_i^{j+1}, \; i = 0,1,...,M, \; j = 0,1,...,N. \tag{12}$$

Now, to linearize the nonlinear term $\left(w^p w_\zeta \right)_i^{j+1}$, we use the Rubin-Graves procedure as:

$$\left(w^p w_\zeta \right)_i^{j+1} \approx \left(w^p \right)_i^j \left(w_\zeta \right)_i^{j+1} + p \left(w^{p-1} \right)_i^j \left(w_\zeta \right)_i^j w_i^{j+1} - p \left(w^p \right)_i^j \left(w_\zeta \right)_i^j + O(\Delta \tau^2), \; p = 1,2,\ldots. \tag{13}$$

Taking $\theta = \frac{1}{2}$ and using Eq (13) in (12) with some manipulation, we have

$$A_i^j w_i^{j+1} + B_i^j \left(w_\zeta\right)_i^{j+1} + D\left(w_{\zeta\zeta}\right)_i^{j+1} = R_i^j,\ i = 0,1,...,M,\ j = 1,2,...,N, \tag{14}$$

where

$$A_i^j = a_0 + \frac{1}{2}\hat{\beta} p\left(w^{p-1}\right)_i^j \left(w_\zeta\right)_i^j,\ \ B_i^j = \frac{1}{2}\hat{\gamma} + \frac{1}{2}\hat{\beta}\left(w^p\right)_i^j,\ \ D = -\frac{\hat{\mu}}{\Delta\tau},\ \ R_i^j = a_0 w_i^j - a_0 \sum_{k=1}^{j} \chi_k \left(w_i^{j-k+1} - w_i^{j-k}\right) - \frac{1}{2}\hat{\gamma}\left(w_\zeta\right)_i^j + \frac{1}{2}\hat{\beta}\, p\left(w^p\right)_i^j \left(w_\zeta\right)_i^j - \frac{1}{2}\hat{\beta}\left(w^p\right)_i^j \left(w_\zeta\right)_i^j + D\left(w_{\zeta\zeta}\right)_i^j + f_i^{j+1}.$$

Next, using the CBS collocation technique, we get

$$\left(\sigma_1 A_i^j - \sigma_3 B_i^j + \sigma_4 D\right) C_{i-1}^{j+1} + \left(\sigma_2 A_i^j - 2\sigma_4 D\right) C_i^{j+1} + \left(\sigma_1 A_i^j + \sigma_3 B_i^j + \sigma_4 D\right) C_{i+1}^{j+1} = R_i^j,$$

$$i = 1,2,...,M-1,\ j = 1,2,...,N, \tag{15}$$

where

$$R_i^j = a_0\left(\sigma_1 C_{i-1}^j + \sigma_2 C_i^j + \sigma_1 C_{i+1}^j\right) - a_0 \sum_{k=1}^{j} \chi_k \left\{\left(\sigma_1 C_{i-1}^{j-k+1} + \sigma_2 C_i^{j-k+1} + \sigma_1 C_{i+1}^{j-k+1}\right) - \left(\sigma_1 C_{i-1}^{j-k} + \sigma_2 C_i^{j-k} + \sigma_1 C_{i+1}^{j-k}\right)\right\} - \frac{1}{2}\hat{\gamma}\left(-\sigma_3 C_{i-1}^j + \sigma_3 C_{i+1}^j\right) + \frac{1}{2}\hat{\beta}\left(-\sigma_3 C_{i-1}^j + \sigma_3 C_{i+1}^j\right) \times \left(\sigma_1 C_{i-1}^j + \sigma_2 C_i^j + \sigma_1 C_{i+1}^j\right)^p (p-1) + D\left(\sigma_4 C_{i-1}^j - 2\sigma_4 C_i^j + \sigma_4 C_{i+1}^j\right) + f_i^{j+1}.$$

The Eq (15) forms a linear system with $M+1$ equations and $M+3$ unknowns. For making it uniquely solvable, we use the boundary conditions $w(a,\tau) = \varphi_1(\tau)$ and $w(b,\tau) = \varphi_2(\tau)$ as

$$\left(\sigma_1 C_{-1}^j + \sigma_2 C_0^j + \sigma_1 C_1^j\right) = \varphi_1^j(\tau), \tag{16}$$

$$\left(\sigma_1 C_{M-1}^j + \sigma_2 C_M^j + \sigma_1 C_{M+1}^j\right) = \varphi_2^j(\tau). \tag{17}$$

From Eqs (16) and (17), we have

$$C_{-1}^j = -\frac{\sigma_2}{\sigma_1} C_0^j - C_1^j + \frac{1}{\sigma_1}\varphi_1^j(\tau) \ \text{ and } \ C_{M+1}^j = -\frac{\sigma_2}{\sigma_1} C_M^j - C_{M-1}^j + \frac{1}{\sigma_1}\varphi_2^j(\tau). \tag{18}$$

For $i = 0$ and $i = M$, inverting the Eq (18) in (15), we get

$$\left(\frac{\sigma_2\sigma_3}{\sigma_1} B_0^j - \frac{\sigma_2}{\sigma_1}\overline{A}_0^j + \overline{B}_0^j\right) C_0^{j+1} + 2\sigma_3 B_0^j C_1^{j+1} = R_0^j - \frac{1}{\sigma_1}\left(\overline{A}_0^j - \sigma_3 B_0^j\right)\varphi_1^{j+1},\ j = 0,1,...,N, \tag{19}$$

and

$$-2\sigma_3 B_M^j C_{M-1}^{j+1} + \left(-\frac{\sigma_2\sigma_3}{\sigma_1} B_M^j - \frac{\sigma_2}{\sigma_1}\overline{A}_M^j + \overline{B}_M^j\right) C_M^{j+1} = R_M^j - \frac{1}{\sigma_1}\left(\overline{A}_M^j + \sigma_3 B_M^j\right)\varphi_2^{j+1},\ \ j = 0,1,...,N, \tag{20}$$

where

$$R_0^j = \left(-\frac{\sigma_2\sigma_3\hat{\gamma}}{2\sigma_1} + \frac{\sigma_2\sigma_3\hat{\beta}}{2\sigma_1}\left(\varphi_i^j\right)^p (p-1) - \frac{\sigma_2\sigma_4 D}{\sigma_1} - 2D\sigma_4\right) C_0^j + \left(\hat{\beta}\sigma_3\left(\varphi_i^j\right)^p (p-1) -$$

$$\hat{\gamma}\sigma_3\big)C_1^j - a_0\sum_{k=1}^{j}\chi_k\left\{\varphi_1^{j-k+1}-\varphi_1^{j-k}\right\}+\left(a_0-\frac{\sigma_3\hat{\gamma}}{2\sigma_1}-\frac{\sigma_3(p-1)\hat{\beta}}{2\sigma_1}\left(\varphi_1^j\right)^p+\frac{\sigma_4}{\sigma_1}\right)\varphi_1^j+f_0^{j+1}.$$

$$R_M^j=\left(\hat{\gamma}\sigma_3-\left(\varphi_2^j\right)^p(p-1)\hat{\beta}\sigma_3\right)C_{M-1}^j+\left(\frac{\sigma_2\sigma_3\hat{\gamma}}{2\sigma_1}-\frac{\sigma_2\sigma_3\hat{\beta}}{2\sigma_1}(p-1)\left(\varphi_2^j\right)^p-\frac{\sigma_2\sigma_4 D}{\sigma_1}+\right.$$

$$\left.2D\sigma_4\big)C_M^j-a_0\sum_{k=1}^{j}\chi_k\left(\varphi_2^{j-k+1}-\varphi_2^{j-k}\right)+\left(a_0+\frac{\sigma_3\hat{\beta}(p-1)}{2\sigma_1}\left(\varphi_2^j\right)^p+\frac{\sigma_4 D}{\sigma_1}-\frac{\sigma_3\hat{\gamma}}{2\sigma_1}\right)\varphi_2^j+f_M^{j+1}.\right.$$

Equations (19), (15) and (20) form the following system of linear equations:

$$\begin{bmatrix}\tilde{A}_0^j & 2\sigma_3B_0^j & 0 & 0 & \cdots & 0\\ \tilde{B}_1^j-\sigma_3B_1^j & \tilde{D}_1^j & \tilde{B}_1^j+\sigma_3B_1^j & 0 & \cdots & 0\\ 0 & \tilde{B}_2^j-\sigma_3B_2^j & \tilde{D}_2^j & \tilde{B}_2^j+\sigma_3B_2^j & \cdots & 0\\ \vdots & \ddots & \ddots & \ddots & \ddots & \vdots\\ 0 & \cdots & 0 & \tilde{B}_{M-1}^j-\sigma_3B_{M-1}^j & \tilde{D}_{M-1}^j & \tilde{B}_{M-1}^j-\sigma_3B_{M-1}^j\\ 0 & \cdots & 0 & 0 & -2\sigma_3B_M^j & \tilde{A}_M^j\end{bmatrix}\begin{bmatrix}C_0^0\\ C_1^0\\ C_2^0\\ \vdots\\ C_{M-1}^0\\ C_M^0\end{bmatrix}=$$

$$\begin{bmatrix}R_0^j-\frac{1}{\sigma_1}\left(\bar{A}_0^j-\sigma_3B_0^j\right)\varphi_1^{j+1}\\ R_1^j\\ R_2^j\\ \vdots\\ R_{M-1}^j\\ R_M^j-\frac{1}{\sigma_1}\left(\bar{A}_M^j+\sigma_3B_M^j\right)\varphi_2^{j+1}\end{bmatrix},\tag{21}$$

where $\tilde{A}_0^j=\frac{\sigma_2\sigma_3}{\sigma_1}B_0^j-\frac{\sigma_2}{\sigma_1}\bar{A}_0^j+\bar{B}_0^j$, $\tilde{B}_i^j=\sigma_1A_i^j+\sigma_4D$, $\tilde{D}_i^j=\sigma_2A_i^j-2\sigma_4D$, and $\tilde{A}_M^j=-\frac{\sigma_2\sigma_3}{\sigma_1}B_M^j-\frac{\sigma_2}{\sigma_1}\bar{A}_M^j+\bar{B}_M^j$.

To solve the system (21), it is necessary to define the initial vector $\left(C_0^0,C_1^0,...,C_{M-1}^0,C_M^0\right)$ from $w(\zeta,0)=\vartheta(\zeta)$ which provides $M+1$ equations with $M+3$ unknowns. To take out C_{-1}^0 and C_{M+1}^0, we use $w_\zeta(a,0)=\vartheta_\zeta(a)$ and $w_\zeta(b,0)=\vartheta_\zeta(b)$ which gives

$$C_{-1}^0=C_1^0-\frac{\vartheta_\zeta(a)}{\tau_3}\quad\text{and}\quad C_{M+1}^0=C_{M-1}^0+\frac{\vartheta_\zeta(b)}{\tau_3}.\tag{22}$$

Now using Eq (22) and the initial condition, we have the subsequent system of linear equations:

$$\begin{bmatrix} \tau_2 & 2\tau_1 & 0 & 0 & \cdots & 0 \\ \tau_1 & \tau_2 & \tau_1 & 0 & \cdots & 0 \\ 0 & \tau_1 & \tau_2 & \tau_1 & \cdots & 0 \\ \vdots & \ddots & \ddots & \ddots & \ddots & \vdots \\ 0 & \cdots & 0 & \tau_1 & \tau_2 & \tau_1 \\ 0 & \cdots & 0 & 0 & 2\tau_1 & \tau_2 \end{bmatrix} \begin{bmatrix} C_0^0 \\ C_1^0 \\ C_2^0 \\ \vdots \\ C_{M-1}^0 \\ C_M^0 \end{bmatrix} = \begin{bmatrix} \vartheta_0 + \left(\vartheta_\zeta\right)_0 \tau_1/\tau_3 \\ \vartheta_1 \\ \vartheta_2 \\ \vdots \\ \vartheta_{M-1} \\ \vartheta_M - \left(\vartheta_\zeta\right)_M \tau_1/\tau_3 \end{bmatrix}. \tag{23}$$

3. Stability analysis

This section establishes the stability for the discretized system of the TFRLW equation using the von Neumann scheme [32]. According to Duhamels' principle [36], the stability of an inhomogeneous system is the same as the stability of the corresponding homogeneous system. Therefore, we choose $f = 0$, and taking $\left(w_\zeta\right)^p = \hat{k}_1^{\,p}$ as locally constant to linearize $w^p w_\zeta$, and $\theta = \frac{1}{2}$, the Eq (12) can be written as

$$a_0 w_i^{j+1} + \frac{1}{2}\left(\hat{\gamma} + \hat{\beta}\hat{k}_1^{\,p}\right)\left(w_\zeta\right)_i^{j+1} - \frac{\hat{\mu}}{\Delta\tau}\left(w_{\zeta\zeta}\right)_i^{j+1} = a_0 \sum_{k=0}^{j-1}\left(\left(\chi_k - \chi_{k+1}\right)\, w_i^{j-k} + \chi_j\, w_i^0\right)$$

$$-\frac{1}{2}\left(\hat{\gamma} + \hat{\beta}\hat{k}_1^{\,p}\right)\left(w_\zeta\right)_i^{j} - \frac{\hat{\mu}}{\Delta\tau}\left(w_{\zeta\zeta}\right)_i^{j},\ i = 0,1,...,M,\ j = 0,1,...,N. \tag{24}$$

With the help of Eqs (9)–(11), we get

$$\left(A^* + E^*\right)C_{i-1}^{j+1} + B^* C_i^{j+1} + \left(A^* - E^*\right)C_{i-1}^{j+1} = a_0 \sum_{k=0}^{j-1}\left(\chi_k - \chi_{k+1}\right)\,\left(\sigma_1 C_{i-1}^{j-k} + \sigma_2 C_i^{j-k} + \sigma_1 C_{i+1}^{j-k}\right)$$

$$+\chi_j\left(\sigma_1 C_{i-1}^0 + \sigma_2 C_i^0 + \sigma_1 C_{i+1}^0\right) + \left(-E^*\sigma_3 - \sigma_4 D\right)C_{i-1}^j + 2\sigma_4 D C_i^j + \left(E^*\sigma_3 - \sigma_4 D\right)C_{i+1}^j, \tag{25}$$

where $A^* = a_0\sigma_1 - \sigma_4 D,\ B^* = a_0\sigma_2 + 2\sigma_4 D,\ D = \frac{\hat{\mu}}{\Delta\tau},$ and $E^* = \frac{1}{2}\left(\hat{\gamma} + \hat{\beta}\hat{k}_1^{\,p}\right).$

Now, using the Fourier mode's growth factor $C_i^j = \xi^j e^{li\varepsilon h}$, where $l = \sqrt{-1}$, ξ is the constraint depending on time, and we have

$$\left(2A^*\cos\varepsilon h + B^* - 2lE^*\sin\varepsilon h\right)\xi^{j+1} = a_0\sum_{k=0}^{j-1}\left(\left(\chi_k - \chi_{k+1}\right)\,\xi^{j-k} + \chi_j\xi^0\right)\left(2\sigma_1\cos\varepsilon h + \sigma_2\right)$$

$$+\left(2\sigma_4 D - 2\sigma_4 D\cos\varepsilon h + 2lE^*\sigma_3\sin\varepsilon h\right)\xi^j. \tag{26}$$

Now, we define $\xi_{\max}^j = \max_{0\le i\le j}\left|\xi^i\right|$.

Using it in the Eq (26), and by means of the property $\sum_{k=0}^{j-1}\left(\left(\chi_k - \chi_{k+1}\right) + \chi_j\right) = 1$, we have

$$|\xi|^2 \leq \frac{S_1}{S_1 + (S_2 - S_1)}, \tag{27}$$

where $S_1 = \left(2a_0\sigma_1 \cos \varepsilon h + a_0\sigma_2 + 2\sigma_4 D - 2\sigma_4 D \cos \varepsilon h\right)^2 + 4E^{*2}\sigma_3{}^2 \sin^2 \varepsilon h$, and $S_2 = \left(2A^* \cos \varepsilon h + B^*\right)^2 + 4E^{*2} \sin^2 \varepsilon h$. Using the values A^*, B^*, D, E^*, σ_1, σ_3, σ_4, and simplifying terms, we have

$$S_2 - S_1 = \left(\frac{4}{h^2}\left(\frac{12}{\overline{|2-\alpha}\,\Delta\tau^{\alpha+1}} - 1\right) + 4\right)\sin^2 \varepsilon h \geq 0. \tag{28}$$

Hence, we conclude that $|\xi| \leq 1$. So, the discretized system of the TFRLW equation is unconditionally stable.

4. Result and discussion

This division provides an example of the TFRLW equation to investigate the efficacy and validation of the projected technique. For this purpose, we use

$$L_2 = \left(\sum_{i=0}^{M} |W(\zeta_i, \tau) - w(\zeta_i, \tau)|^2\right)^{1/2}, \quad L_\infty = \max_{0 \leq i \leq M} |W(\zeta_i, \tau) - w(\zeta_i, \tau)_j|,$$

and approximate error = $\dfrac{|w(\zeta_j, \tau_{N+1}) - w(\zeta_i, \tau_N)|}{|w(\zeta_j, \tau_{N+1})|}$,

where W represents the exact solution. The ROC is analyzed by $\mathrm{ROC} = \dfrac{\ln\left(err(h_1)/err(h_2)\right)}{\ln\left(h_1/h_2\right)}$, where the terms $err(h_1)$ and $err(h_2)$ represents errors with h_1 and h_2, in that order. The conservation possessions belonging to the TFRLW equation are measured by calculating quantities analogous to mass, momentum, and energy, respectively, as follows:

$$I_1 = \int_a^b w d\zeta \cong h\sum_{i=0}^{M} W_i, \tag{29}$$

$$I_2 = \int_a^b \left(w^2 + \hat{\mu}\left(w_\zeta\right)^2\right) d\zeta \cong h\sum_{i=0}^{M}\left(\left(W_i\right)^2 + \hat{\mu}\left(W_\zeta\right)_i{}^2\right), \tag{30}$$

$$I_3 = \int_a^b \left(w^3 + 3\left(w_\zeta\right)^2\right) d\zeta \cong h\sum_{i=0}^{M}\left(\left(W_i\right)^3 + 3\left(W_\zeta\right)_i{}^2\right). \tag{31}$$

Now, we consider the TFRLW equation (1) with $\hat{\gamma} = 1 = \hat{\beta} = \hat{\mu} = p$ together with initial and boundary conditions $w(\zeta, 0) = 3\rho \sec h^2(\eta\zeta)$ and $w(a, \tau) = w(b, \tau) = 0$. Here, 3ρ is the amplitude and $\eta = \dfrac{1}{2}\sqrt{\dfrac{\rho}{1+\rho}}$. When α =1, the TFRLW equation has the subsequent single solitary wave solution

$w(\zeta,\tau)=3\rho\sec h^2(\eta\zeta-\varpi\tau+\zeta_0)$, where $\varpi=\frac{1}{2}\sqrt{\rho(1+\rho)}$, ζ_0 is an arbitrary constant, and η and ϖ/η represent the width and velocity, respectively. For all calculations, we have chosen $\zeta_0=0$.

Figure 1 signifies the estimated solution $w(\zeta,\tau)$ with admiration of the time τ for several values of ρ. From this figure, it can be revealed that the estimated solution $w(\zeta,\tau)$ increases as the value of ρ increases. The approximate solutions with $h=0.4$, $\Delta\tau=0.01$, $\rho=0.03$ at times $\tau=5$, 7, 10 and 20 are demonstrated in Figure 2 for time-fractional orders $\alpha=0.3$, 0.5, 0.7, and 0.8. The figures show the influence of the Caputo order α of the fractional derivative on the evolution of the obtained solutions over time. An apparent dependence of α on the solutions can be seen clearly when the time is large. Table 2 shows the approximate errors together with an ROC for $\alpha=0.9$ with $\rho=0.1$, $h=0.2$, and $\tau=0.1$ with respect to various time intervals. It can be perceived that the errors are very small and the projected method is linearly convergent with respect to the time variable. Table 3 shows the approximate errors for $\alpha=0.4$ with $\rho=0.03$, $h=0.2$, $\zeta=2$ and 4 for various time intervals at $\tau=1$ while Table 4 illustrates the approximate errors with $\rho=0.1$, $h=0.2$ for fractional orders $\alpha=0.5$, and 0.7 at times $\tau=5$ and 10. It can be noticed from these tables that the approximate errors are small which confirms the accuracy of the proposed technique.

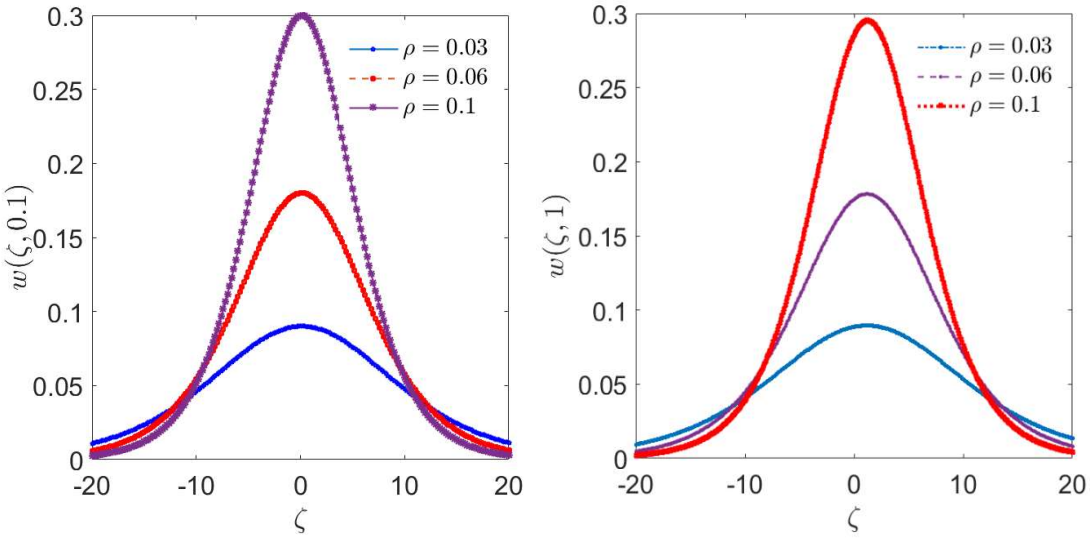

Figure 1. The approximate solutions comportment for distinctive values of ρ with $h=0.1$, $\Delta\tau=0.01$ for $\alpha=0.9$ (left) and $\alpha=0.5$ (right) of Example 1.

Table 2. The approximate errors for $\alpha=0.9$ with $\rho=0.1$, $h=0.2$, and $\tau=0.1$ for various time intervals.

$\Delta\tau$	$\zeta=2$	ROC	$\zeta=4$	ROC
0.05	2.08570e-04	--	4.03268e-04	--
0.001	1.04198e-04	1.0010	2.01542e-04	1.0006
0.0005	5.20759e-05	1.0006	1.00746e-04	1.0004
0.00025	2.60318e-05	1.0003	5.03664e-05	1.0002
0.0002	2.08245e-05	1.0002	4.02919e-05	1.0001
0.000125	1.30143e-05	1.0001	2.51814e-05	1.000
0.00001	1.04112e-05	1.0001	2.01448e-05	1.000

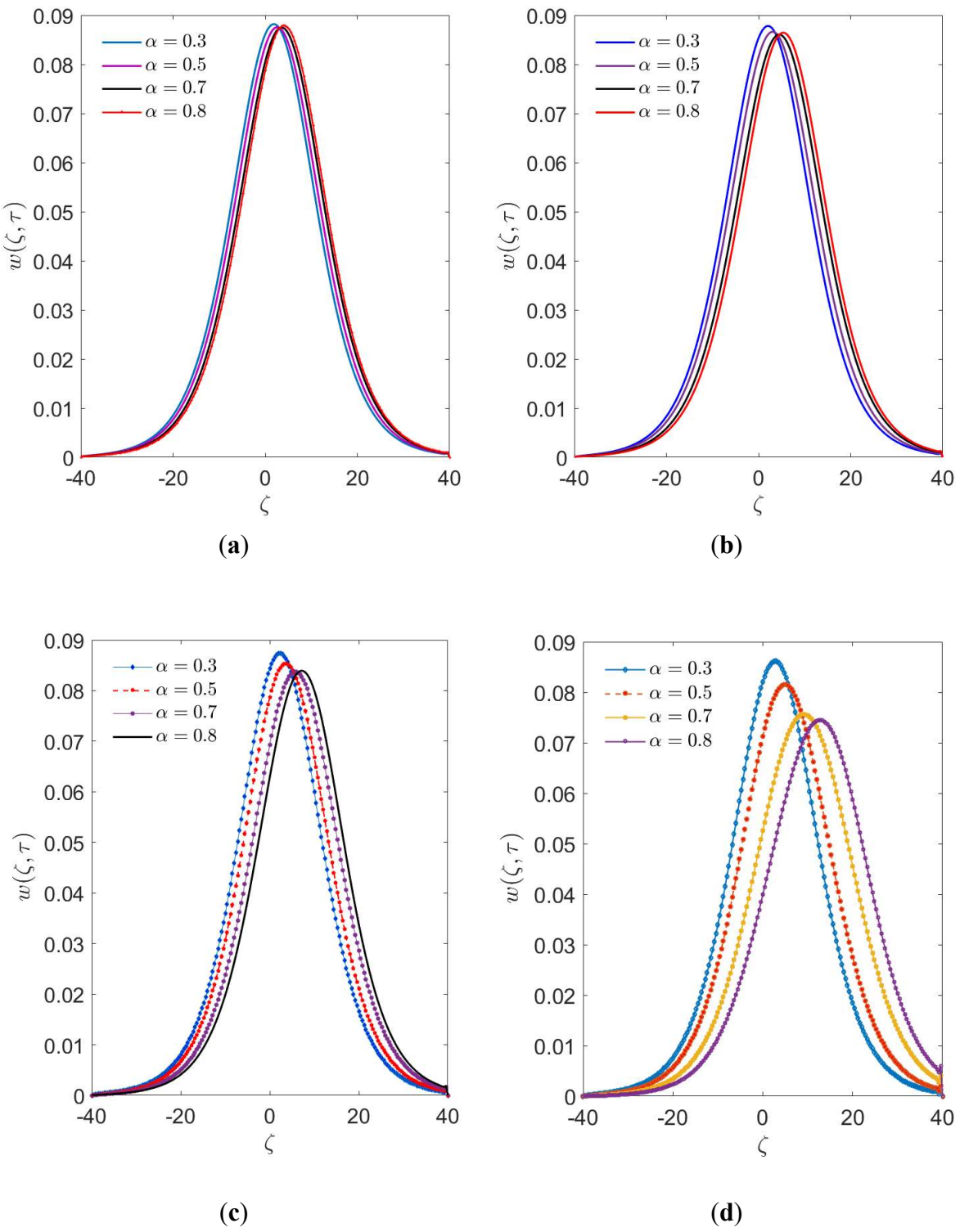

Figure 2. The approximate solutions with $h = 0.4$, $\Delta\tau = 0.01$, $\rho = 0.03$ at times (a) $\tau = 5$, (b) $\tau = 7$, (c) $\tau = 10$, and (d) $\tau = 20$ (right) for different values of fractional order α for Example 1.

Table 3. The approximate errors for $\alpha = 0.4$ with $\rho = 0.03$, $h = 0.2$, and $\tau = 1$ for various time intervals.

$\Delta\tau$	$\zeta = 2$	ROC	$\zeta = 4$	ROC
0.05	3.126e-05	--	7.786e-04	--
0.025	1.181e-05	1.40	3.791e-04	1.04
0.0125	5.020e-06	1.23	1.870e-04	1.02
0.01	3.879e-06	1.56	1.493e-04	1.01
0.008	3.017e-06	1.13	1.192e-04	1.01
0.00625	2.299e-06	1.10	9.295e-05	1.01

Table 4. The approximate errors with $\rho = 0.1$, $h = 0.2$, and $\tau = 10$ at $\zeta = 4$ for various time intervals.

$\Delta\tau$	$\alpha = 0.5,\ \tau = 5$	$\alpha = 0.5,\ \tau = 10$	$\alpha = 0.7,\ \tau = 5$	$\alpha = 0.7,\ \tau = 10$
0.05	3.0576e-04	5.9194e-04	1.1811e-03	2.0957e-03
0.025	1.5319e-04	2.9497e-04	5.9586e-04	1.0434e-03
0.0125	7.6638e-05	1.4723e-04	2.9914e-04	5.2055e-04
0.01	6.1314e-05	1.1775e-04	2.3950e-04	4.1626e-04
0.008	4.9054e-05	9.4173e-05	1.9171e-04	3.3289e-04
0.001	3.0660e-05	5.8834e-05	1.1992e-04	2.0794e-04

Table 5 shows the ROC with respect to the space variable including errors in invariants for $\alpha = 1$ with $\rho = 0.1$, $\Delta\tau = 0.01$ at $\tau = 1$. It can be noticed from this table that the projected method is second-order convergent in space as well as that the small difference among the numerical and analytical values of I_1, I_2, and I_3 that extends in the invariants remains almost inconsistent for the duration of the computer run.

Table 5. The order of convergence including errors on invariants for $\alpha = 1$ with $\rho = 0.1$, $\Delta\tau = 0.01$, at $\tau = 1$.

h	L_2	ROC	L_∞	ROC	ΔI_1	ΔI_2	ΔI_3
0.8	1.232e-04	--	5.282e-05	--	1.324e-05	4.253e-07	1.982e-09
0.5	4.675e-05	2.06	2.023e-05	2.04	1.358e-05	3.550e-08	1.253e-10
0.4	2.976e-05	2.02	1.295e-05	2.00	1.369e-05	3.645e-09	3.864e-11
0.25	1.166e-05	1.99	5.050e-06	2.00	1.389e-05	5.448e-09	2.081e-12
0.2	7.558e-06	1.94	3.235e-06	1.99	1.389e-05	5.448e-09	2.081e-12
0.125	3.290e-06	1.77	1.725e-06	1.34	1.397e-05	2.662e-09	1.059e-12

Table 6 demonstrates a comparison between the projected method and those available in refs. [18,19,33,34] in terms of L_2 and L_∞ errors. The values of the single solitary wave's invariants are also compared for $\alpha = 1$ with $\rho = 0.1$, $h = 0.125$, $\Delta\tau = 0.1$, and $\zeta \in [-40, 60]$ at various times. It is observed from Table 6 that the magnitudes in the invariants keep almost insistent in the course of the computer run. At $\tau = 16$, the difference among the numerical and analytical values of the conservation constants are $\Delta I_1 = 4.815941\text{e-}05$, $\Delta I_2 = 1.856193\text{e-}06$, $\Delta I_3 = 2.651635\text{e-}08$. It

is obvious from the table that the L_∞ error norms at each time achieved by the projected method are much lower than those given in refs. [18,19,33,34], However, the L_2 error norm is only higher than in [18] and is lower than the others. Also, the L_2 and L_∞ errors in [33] are slightly smaller than those achieved by the projected method.

Table 6. Invariants with L_2 and L_∞ errors for the single solitary wave for $\alpha = 1$ with $\rho = 0.1$, $h = 0.125$, $\Delta\tau = 0.1$, $\zeta \in [-40, 60]$ at various times.

Time	Methods	L_2	L_∞	I_1	I_2	I_3
$\tau = 4$	Present	5.279e-05	2.118e-05	3.979955	0.810463	2.579007
	Ref. [33]	4.8e-05	1.9e-05	3.97993	0.810465	2.57901
	Ref. [19]	1.09e-03	4.87e-04	3.98041	0.810111	2.57785
	Ref. [18]	1.00e-05	1.46e-04	3.97709	0.809641	2.57630
	Ref. [34]	1.16e-04	5.4e-05	3.98039	0.810610	2.57950
$\tau = 8$	Present	1.05e-04	4.252e-05	3.979976	0.810463	2.579007
	Ref. [33]	9.4e-05	3.8e-05	3.97993	0.810465	2.57901
	Ref. [19]	2.109e-03	8.92e-04	3.98085	0.809749	2.57666
	Ref. [18]	3.0e-06	5.79e-04	3.97332	0.808320	2.57194
	Ref. [34]	2.24e-04	1.00e-04	3.98083	0.810752	2.57996
τ =12	Present	1.5395e-04	6.216e-05	3.9799927	0.810463	2.579007
	Ref. [33]	1.38e-04	5.6e-05	3.97992	0.810465	2.57901
	Ref. [19]	3.049e-03	1.224e-03	3.98128	0.809390	2.57547
	Ref. [18]	6.0e-06	9.22e-04	3.97911	0.806774	2.56684
	Ref. [34]	3.25e-04	1.39e-04	3.98125	0.810884	2.58041
τ =16	Present	2.012e-04	7.994e-05	3.979997	0.810464	2.579007
	Ref. [33]	1.80e-04	7.1e-05	3.97991	0.810465	2.57901
	Ref. [19]	3.905e-03	1.510e-03	3.98169	0.809030	2.57428
	Ref. [18]	1.2e-05	1.215e-03	3.96534	0.805461	2.56251
	Ref. [34]	4.17e-04	1.71e-04	3.98165	0.811014	2.58083

Table 7 compares the projected method and existing methods refs. [19,23,33,34,37] in terms of L_2 and L_∞ errors as well as invariants for $\alpha = 1$ with $\rho = 0.1$, $h = 0.125$, $\Delta\tau = 0.1$, and $\zeta \in [-40, 60]$ at time $\tau = 20$. It can be perceived from this table that the L_2 and L_∞ error norms achieved by the projected method are very much smaller than those obtained in [19,23,33,34,37], whereas, the errors obtained by the QBGM1 are almost similar to the projected method. The magnitudes in the invariants keep on nearly consistent in the course of the computer run. It is found that the difference among the numerical and analytical values of I_1, I_2, and I_3 are $\Delta I_1 = 2.496862$e-

05, ΔI_2= 2.642822e-06, and ΔI_3= 3.886086e-08. Table 8 compares the invariants obtained by the projected method with ref. [37] and analytical quantities for $\alpha = 0.5$ with $\rho = 0.03$, $h = 0.1$, $\Delta\tau$= 0.0001 at various times τ. It can be remarked from this table that the obtained invariant quantities are very close to analytical values and are much better than what is presented in ref. [37]. Table 9 shows the absolute errors in the invariants obtained by the projected method and analytical quantities for α = 0.6 with $\rho = 0.03$, $h = 0.2$, $\Delta\tau = 0.001$ at various times τ. It can be seen that the invariant quantities are nearly 10^{-3} accurate.

Table 7. The comparison of L_2 and L_∞ errors and invariants obtained by the projected method and existing methods for $\alpha = 1$ with $\rho = 0.1$, $h = 0.125$, $\Delta\tau$= 0.1, $\zeta \in [-40, 60]$ at $\tau = 20$.

Methods	L_2	L_∞	I_1	I_2	I_3
Present	2.4627e-04	9.6078e-05	3.979975	0.810465	2.579007
Ref. [19]	4.688e-03	1.755e-03	3.98203	0.808650	2.57302
Ref. [37]	2.20e-04	8.60e-05	3.97989	0.810467	2.57902
Ref. [33]	2.19e-04	8.60e-05	3.97988	0.810465	2.57901
QBGM1 (Ref. [23])	1.9215e-04	7.337e-05	3.9798832	0.8104612	2.5790031
QBGM2 (Ref. [23])	3.5489e-04	1.2848e-04	3.9798830	0.8104616	2.5790043
Ref. [34]	5.11e-04	1.98e-04	3.98206	0.811164	2.58133

Table 8. The comparison of invariants obtained by the projected method with ref. [37] and analytical quantities for $\alpha = 0.5$ with $\rho = 0.03$, $h = 0.1$, $\Delta\tau = 0.0001$ at various times τ.

τ	Methods	I_1	I_2	I_3
0.01	Present	2.104795105493023	0.127311100687075	0.388792279082409
	Exact values	2.109407499749634	0.127301718625667	0.388805990353852
	Ref. [37]	0.197709389335031	0.126849748687847	0.387166785333068
0.02	Present	2.104793676163467	0.127306603010193	0.388778144598822
	Exact values	2.109407499749634	0.127301718625667	0.388805990353852
	Ref. [37]	0.197709389335031	0.126832805997773	0.387113999130940
0.03	Present	2.104792339908470	0.127301823129927	0.388763112448558
	Exact values	2.109407499749634	0.127301718625667	0.388805990353852
	Ref. [37]	0.197705310408835	0.126802946718958	0.387058367254051
0.04	Present	2.104791052954834	0.127296885458673	0.388747577127724
	Exact values	2.109407499749634	0.127301718625667	0.388805990353852
	Ref. [37]	0.197698761277219	0.126780218019371	0.387001260827619
0.05	Present	2.104789799868593	0.127291842792910	0.388731706486992
	Exact values	2.109407499749634	0.127301718625667	0.388805990353852
	Ref. [37]	0.197690652584066	0.126757804752181	0.386943215828569

Table 9. The absolute errors in invariants obtained by the projected method and analytical quantities for $\alpha = 0.6$ with $\rho = 0.03$, $h = 0.2$, $\Delta\tau = 0.001$ at various times τ.

τ	I_1	I_2	I_3
0.01	4.750272418178e-03	3.379346449474130e-04	1.087110202561e-03
0.02	4.755032046523e-03	3.758097931880755e-04	1.206502603342e-03
0.03	4.756680570585e-03	3.896019672482709e-04	1.249979299056e-03
0.04	4.757509362131e-03	3.967863361757640e-04	1.272626452249e-03
0.05	4.758004486260e-03	4.012071170268194e-04	1.286562027427e-03

Figure 3 demonstrates the plots of the estimate solution $w(\zeta,\tau)$ contrasted with spatial as well as time variables ζ and τ, respectively, for the values of $\alpha = 0.5$ and $\alpha = 0.75$ showing that the appearances of this figure are stable with ref. [35] (Figures 2 and 3). Figure 4 illustrates the approximate errors for $\alpha = 0.5$ with $\rho = 0.1$, $h = 0.1$ for various time interval sizes $\Delta\tau$ at $\tau = 0.1$. It can be seen from this figure that the approximate errors are decreasing on increasing $\Delta\tau$. Also, it is observed that the approximate errors are less than 10^{-5} which shows the accuracy of the projected method. The 3D plot of the approximate errors for $\alpha = 0.9$ with $\rho = 0.1$, $h = 0.2$, $\Delta\tau = 0.001$, and $\tau \in [0, 0.1]$ is depicted in Figure 5. The depiction of single solitary wave solutions with absolute errors by assuming $\alpha = 1$, $h = 0.3$, $\Delta\tau = 0.1$ for $\rho = 0.1$ and $\rho = 0.03$ at $\tau = 1$ is described in Figure 6.

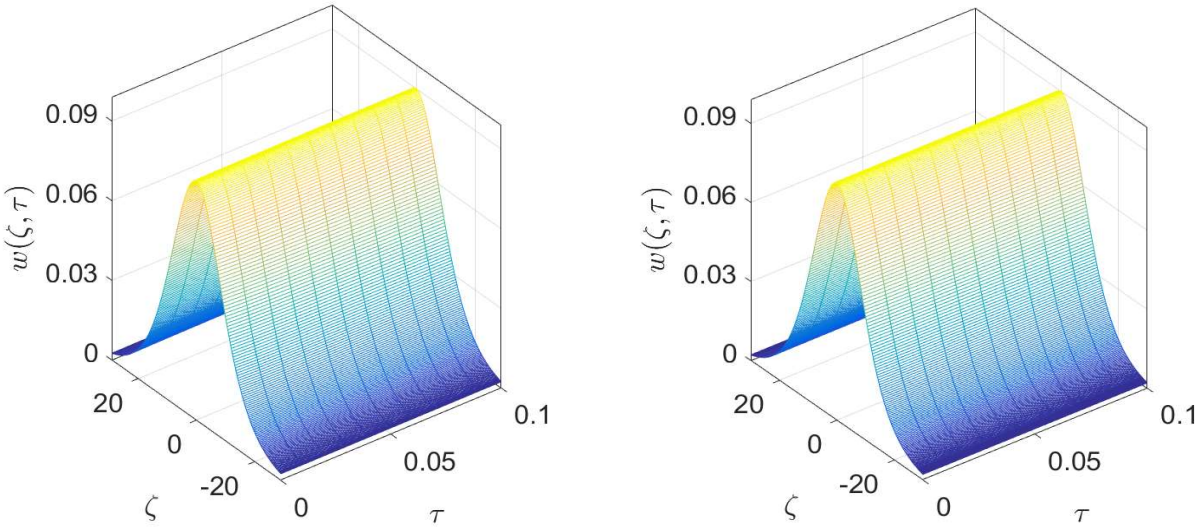

Figure 3. The surface behaviors of the numerical $w(\zeta,\tau)$ for $\alpha = 0.5$ (left), and $\alpha = 0.75$ (right) with $\rho = 0.3$, $h = 0.2$, $\tau \in [0, 0.1]$, and $\Delta\tau = 0.01$ for Example 1.

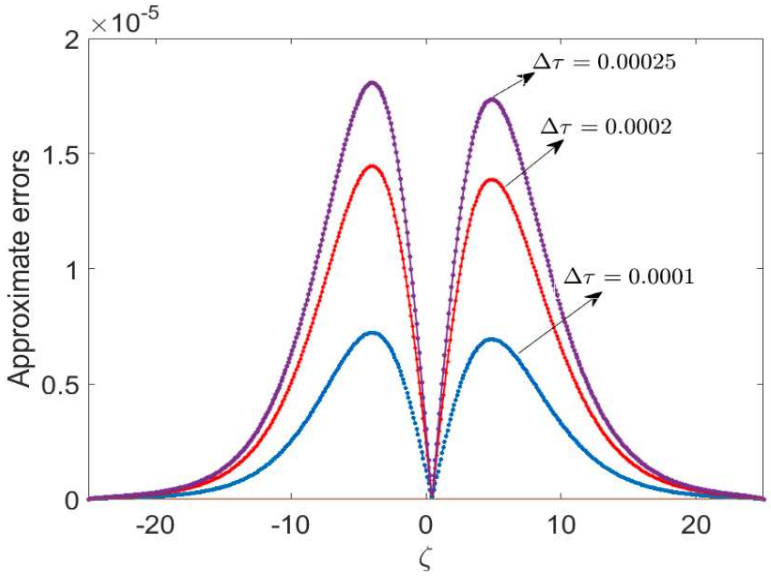

Figure 4. The approximate errors for $\alpha = 0.5$ with $\rho = 0.1$, $h = 0.1$ for various $\Delta\tau$ at $\tau = 0.1$.

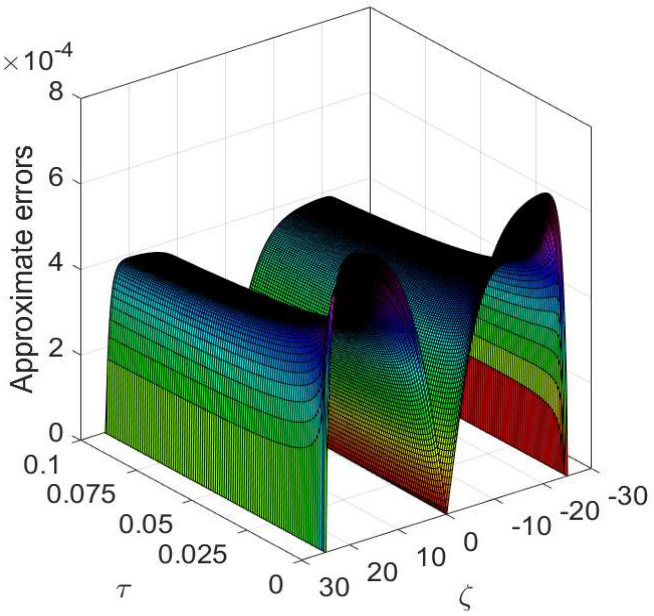

Figure 5. The 3D plot of the approximate errors for $\alpha = 0.9$ with $\rho = 0.1$, $h = 0.2$, $\Delta\tau = 0.001$, and $\tau \in [0, 0.1]$.

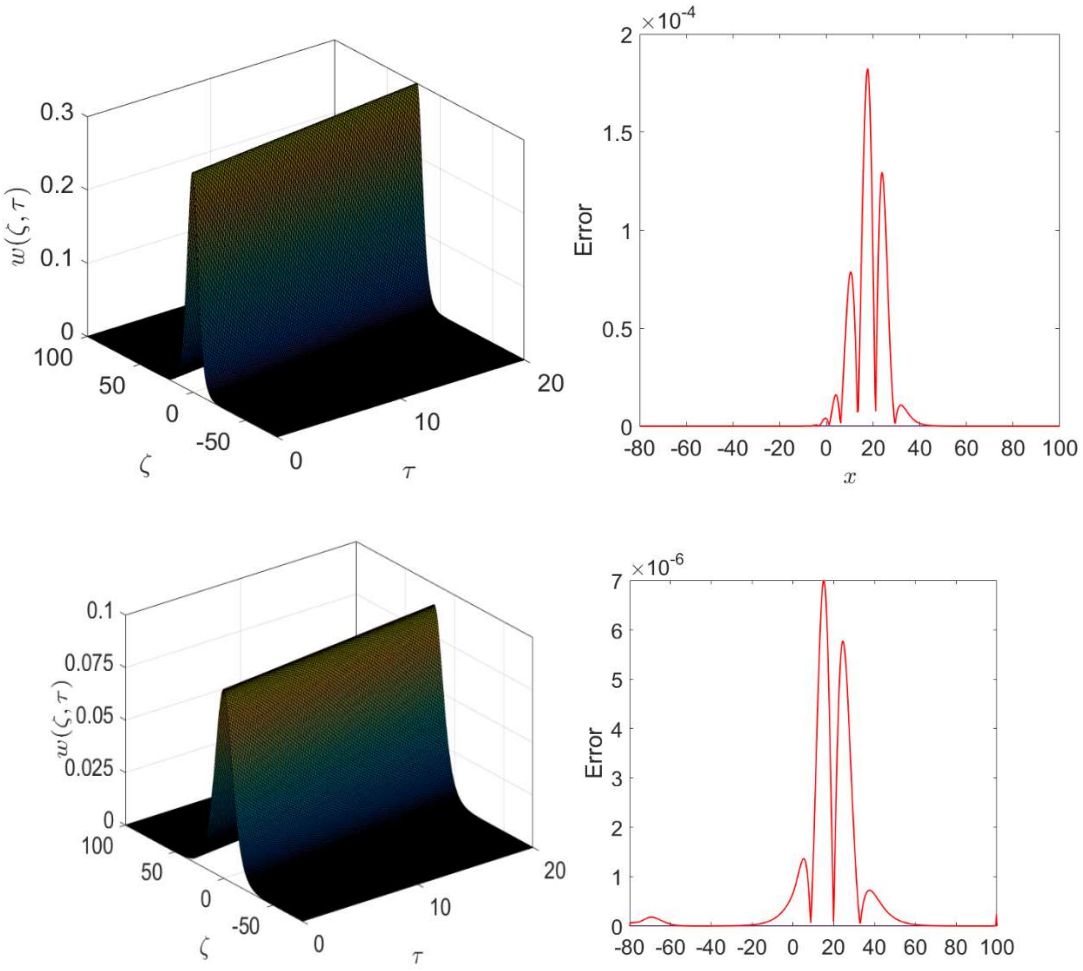

Figure 6. The single solitary wave solutions' performance with absolute errors with $\alpha = 1$, $h = 0.3$, $\Delta\tau = 0.1$ for $\rho = 0.1$ (up) and $\rho = 0.03$ (down) at $\tau = 1$.

5. Conclusions

The traveling-wave solutions are obtained for the TFRLW equation via a CBS collocation technique. The spatial derivatives are discretized by the aforesaid technique while the time-fractional derivative is discretized through Caputo's definition. The nonlinear term is commenced by the Rubin-Graves linearization procedure. The von-Neumann analysis confirms that the discretized structure of the TFRLW equation is enthusiastically stable. It is also established that the technique is second-order convergent in the spatial variable while linearly convergent in time. Three invariant capacities corresponding to mass, momentum, and energy are assessed for further justification. It is demonstrated that these invariants remain almost inconsistent for the duration of the computer run, and absolute errors are very small, approximately $\approx 10^{-8}$ to 10^{-5}. It is also observed that the obtained results by the projected technique are much better than the existing ones in [18,19,23,33,34,37].

Author contributions

All authors of this article have been contributed equally. All authors have read and approved the final version of the manuscript for publication.

Use of Generative-AI tools declaration

The authors declare they have not used Artificial Intelligence (AI) tools in the creation of this article.

Acknowledgments

The authors gratefully acknowledge the funding of the Deanship of Graduate Studies and Scientific Research, Jazan University, Saudi Arabia, through project number RG24-S011.

Conflict of interest

There is no competing interest among the authors regarding the publication of the article.

References

1. D. H. Peregrine, Calculations of the development of an undular bore, *J. Fluid Mech.*, **25** (1966), 321–330. https://doi.org/10.1017/S0022112066001678
2. J. L. Bona, P. J. Bryant, A mathematical model for long waves generated by wave makers in non -linear dispersive systems, *Math. Proc. Cambridge*, **73** (1973), 391–405. https://doi.org/10.1017/S0305004100076945
3. T. B. Benjamin, J. L. Bona, J. J. Mahony, Model equations for long waves in non-linear dispersive systems, *Philos. T. Roy. Soc. A*, **272** (972), 470–478.
4. J. L. Bona, W. G. Pritchard, L. R. Scott, An evaluation of a model equation for water waves, *Philos. T. Roy. Soc. A*, **302** (1981), 457–510. https://doi.org/10.1098/rsta.1981.0178
5. I. Podlubny, *Fractional differential equations*, Academic Press, San Diego, 1999.
6. O. Nikan, J. A. T. Machado, A. Golbabai, T. Nikazad, Numerical approach for modeling fractal mobile/immobile transport model in porous and fractured media, *Int. Commun. Heat Mass*, **111** (2020), 104443. https://doi.org/10.1016/j.icheatmasstransfer.2019.104443
7. A. Golbabai, O. Nikan, T. Nikazad, Numerical investigation of the time fractional mobile-immobile advection-dispersion model arising from solute transport in porous media, *Int. J. Appl. Comput. Math*., **5** (2019), 1–22. https://doi.org/10.1007/s40819-019-0635-x
8. D. Kumar, J. Singh, D. Baleanu, A new analysis for fractional model of regularized long-wave equation arising in ion acoustic plasma waves, *Math. Method. Appl. Sci*., **40** (2017), 5642–5653. https://doi.org/10.1002/mma.4414
9. D. Kumar, J. Singh, D. Baleanu, Sushila, Analysis of regularized long-wave equation associated with a new fractional operator with Mittag-Leffler type kernel, *Physica A*, **492** (2018), 155–167. https://doi.org/10.1016/j.physa.2017.10.002
10. W. Zhang, X. Cai, S. Holm, Time-fractional heat equations and negative absolute temperatures, *Comput. Math. Appl.*, **67** (2014), 164–171. https://doi.org/10.1016/j.camwa.2013.11.007
11. F. A. Rihan, D. Baleanu, S. Lakshmanan, R. Rakkiyappan, On fractional SIRC model with salmonella bacterial infection, *Abstr. Appl. Anal.*, **2014** (2014), 1–9. https://doi.org/10.1155/2014/136263
12. K. Diethelm, N. J. Ford, A. D. Freed, A predictor-corrector approach for the numerical solution of fractional differential equations, *Nonlinear Dyn.*, **29** (2002), 3–22. https://doi.org/10.1023/A:1016592219341

13. L. Debnath, Recent applications of fractional calculus to science and engineering, *Int. J. Math. Math. Sci.*, **2003** (2003), 3413–3442. https://doi.org/10.1155/S0161171203301486
14. A. Padder, L. Almutairi, S. Qureshi, A. Soomro, A. Afroz, E. Hincal, et al., Dynamical analysis of generalized Tumor model with Caputo fractional-order derivative, *Fractal Fract.,* **7** (2023), 258. https://doi.org/10.3390/fractalfract7030258
15. J. C. Eilbeck, G. R. McGuire, Numerical study of the regularized long wave equation I: numerical methods, *J. Comput. Phys.,* **19** (1975), 43–57. https://doi.org/10.1016/0021-9991(75)90115-1
16. P. C. Jain, R. Shankar, T. V. Singh, Numerical solutions of RLW equation, *Commun. Numer. Meth. Eng.*, **9** (1993), 587–594. https://doi.org/10.1002/cnm.1640090705
17. P. Avilez-Valente, F. J. Seabra-Santos, A Petrov-Galerkin finite element scheme for the regularized long wave equation, *Comput. Mech.*, **34** (2004), 256–270. https://doi.org/10.1007/s00466-004-0570-4
18. L. R. T. Gardner, G. A. Gardner, A. Dogan, A least-squares finite element scheme for the RLW equation, *Commun. Numer. Meth. Eng.*, **12** (1996), 795–804. https://doi.org/10.1002/(SICI)1099-0887(199611)12:11<795::AID-CNM22>3.0.CO;2-O
19. İ. Dağ, M. N. Özer, Approximation of the RLW equation by the least square cubic B-spline finite element method, *Appl. Math. Model.*, **25** (2001), 221–231. https://doi.org/10.1016/S0307-904X(00)00030-5
20. I. Dag, Least squares quadratic B-spline finite element method for the regularized long wave equation, *Comput. Method. Appl. M.*, **182** (2000), 205–215. https://doi.org/10.1016/S0045-7825(99)00106-1
21. S. I. Zaki, Solitary waves of the splitted RLW equation, *Comput. Phys. Commun.*, **138** (2001), 80–91. https://doi.org/10.1016/S0010-4655(01)00200-4
22. B. Saka, İ. Dağ, A. Doğan, Galerkin method for the numerical solution of the RLW equation using quadratic B-splines, *Int. J. Comput. Math.*, **81** (2004), 727–739. https://doi.org/10.1080/00207160310001650043
23. İ. Dağ, B. Saka, D. Irk, Galerkin method for the numerical solution of the RLW equation using quintic B-splines, *J. Comput. Appl. Math.*, **190** (2006), 532–547. https://doi.org/10.1016/j.cam.2005.04.026
24. S. Kutluay, A. Esen, A finite difference solution of the regularized long-wave equation, *Math. Prob. Eng.*, **2006** (2006), 1–14. https://doi.org/10.1155/MPE/2006/85743
25. K. R. Raslan, A computational method for the regularized long wave (RLW) equation, *Appl. Math. Comput.*, **167** (2005), 1101–1118. https://doi.org/10.1016/j.amc.2004.06.130
26. İ. Dağ, A. DoĞan, B. Saka, B-Spline collocation methods for numerical solutions of the RLW equation, *Int. Comput. Math.*, **80** (2003), 743–757. https://doi.org/10.1080/0020716021000038965
27. B. Saka, İ. Dağ, Quartic B-spline collocation algorithms for numerical solution of the RLW equation, *Numer. Meth. Part. D. E.*, **23** (2007), 731–751. https://doi.org/10.1002/num.20201
28. M. Tamsir, M. J. Huntul, N. Dhiman, S. Singh, Redefined quintic B-spline collocation technique for nonlinear higher order PDEs, *Comp. Appl. Math.*, **41** (2022), 413. https://doi.org/10.1007/s40314-022-02127-3
29. R. C. Mittal, R. Rohila, A fourth order cubic B-spline collocation method for the numerical study of the RLW and MRLW equations, *Wave Motion*, **80** (2018), 47–68. https://doi.org/10.1016/j.wavemoti.2018.04.001
30. A. Korkmaz, İ. Dağ, Numerical simulations of boundary-forced RLW equation with cubic B-spline-based differential quadrature methods, *Arab. J. Sci. Eng.*, **38** (2013), 1151–1160. https://doi.org/10.1007/s13369-012-0353-8
31. S. G. Rubin, R. A. Graves, Viscous flow solutions with a cubic spline approximation, *Comput. Fluids*, 1975. https://doi.org/10.1016/0045-7930(75)90006-7

32. P. Roul, A high accuracy numerical method and its convergence for time-fractional Black-Scholes equation governing European options, *Appl. Numer. Math.*, **151** (2020), 472–493. https://doi.org/10.1016/j.apnum.2019.11.004
33. A. Esen, S. Kutluay, Application of a lumped Galerkin method to the regularized long wave equation, *Appl. Math. Comput.*, **174** (2006), 833–845. https://doi.org/10.1016/j.amc.2005.05.032
34. A. Dogan, Numerical solution of RLW equation using linear finite elements within Galerkin's method, *Appl. Math. Model.*, **26** (2002), 771–783. https://doi.org/10.1016/S0307-904X(01)00084-1
35. O. Nikan, S. M. Molavi-Arabshai, H. Jafari, Numerical simulation of the nonlinear fractional regularized long-wave model arising in ion acoustic plasma waves, *Discrete Cont. Dyn.-S*, **14** (2021), 3685–3701. https://doi.org/10.3934/dcdss.2020466
36. J. C. Strikwerda, *Finite difference schemes and partial differential equations*, 2 Eds., 2004, SIAM. https://doi.org/10.1137/1.9780898717938
37. L. R. T. Gardner, G. A. Gardner, I. Dag, A B-spline finite element method for the regularized long wave equation, *Commun. Numer. Meth. Eng.*, **11** (1995), 59–68. https://doi.org/10.1002/cnm.1640110109
38. N. Maarouf, H. Maadan, K. Hilal, Lie symmetry analysis and explicit solutions for the time-fractional regularized long-wave equation, *Int. J. Differ. Eq.*, **2021** (2021), 1–11. https://doi.org/10.1155/2021/6614231
39. M. Naeem, H. Yasmin, R. Shah, N. A. Shah, K. Nonlaopon, Investigation of fractional nonlinear Regularized Long-Wave models via novel techniques, *Symmetry*, **15** (2023), 220. https://doi.org/10.3390/sym15010220
40. S. Hossain, M. M. Roshid, M. Uddin, A. A. Ripa, H. O. Roshid, Abundant time-wavering solutions of a modified regularized long wave model using the EMSE technique, *Part. Differ. Eq. Appl. Math.*, **8** (2023), 100551. https://doi.org/10.1016/j.padiff.2023.100551
41. A. Goswami, J. Singh, D. Kumar, S. Gupta, Sushila, An efficient analytical technique for fractional partial differential equations occurring in ion acoustic waves in plasma, *J. Ocean Eng. Sci.*, **4** (2019), 85–99. https://doi.org/10.1016/j.joes.2019.01.003
42. A. Podder, M. A. Arefin, M. A. Akbar, M. H. Uddin, A study of the wave dynamics of the space–time fractional nonlinear evolution equations of beta derivative using the improved Bernoulli sub-equation function approach, *Sci. Rep.*, **13** (2023), 20478. https://doi.org/10.1038/s41598-023-45423-6
43. S. Behera, Analysis of traveling wave solutions of two space-time nonlinear fractional differential equations by the first-integral method, *Mod. Phys. Lett. B*, **38** (2024), 235024. https://doi.org/10.1142/S0217984923502470
44. İ. Yalçınkaya, H. Ahmad, O. Tasbozan, A. Kurt, Soliton solutions for time fractional ocean engineering models with Beta derivative, *J. Ocean Eng. Sci.*, **7** (2022), 444–448. https://doi.org/10.1016/j.joes.2021.09.015
45. M. N. Alam, M. A. Rahman, Study of the parametric effect of the wave profiles of the time –space fractional soliton neuron model equation arising in the topic of neuroscience, *Part. Differ. Equat. Appl. Math.*, **12** (2024), 100985. https://doi.org/10.1016/j.padiff.2024.100985